

# Shadows of Charged and Rotating Black Holes with a Cosmological Constant

A. Belhaj<sup>1,\*</sup>, M. Benali<sup>1</sup>, A. El Balali<sup>1</sup>, W. El Hadri<sup>1</sup>, H. El Moumni<sup>2,†</sup>

<sup>1</sup> Département de Physique, Equipe des Sciences de la matière et du rayonnement, ESMaR

Faculté des Sciences, Université Mohammed V de Rabat, Rabat, Morocco

<sup>2</sup> EPTHE, Physics Department, Faculty of Science, Ibn Zohr University, Agadir, Morocco

January 17, 2022

## Abstract

Motivated by recent astrophysical observations, we investigate the shadow behaviors of four dimensional charged rotating black holes with a cosmological constant. This study is made in terms of a reduced moduli space parameterized by the charge and the rotation parameters. For a negative cosmological constant, we analyse in some details two models dealing with Kerr-Newman and Kerr-Sen black holes. In certain parameter regions, we find cardioid-like (heart-shaped) shadows. For Anti de Sitter backgrounds, a comparative discussion is provided by computing the geometrical observables and the energy emission rate. Inspecting the effect of the cosmological constant, we obtain conditions favoring cardioid-like shadows for (Anti) de Sitter spaces.

**Keywords:** Charged and rotating black holes, Cosmological constant, Shadows, Observable.

---

\*belhajadil@fsr.ac.ma

†hasan.elmoumni@edu.uca.ma

‡Authors in alphabetical order.

# Contents

<b>1</b>	<b>Introduction</b>	<b>2</b>
<b>2</b>	<b>Shadows of Kerr-Newman AdS black hole</b>	<b>3</b>
<b>3</b>	<b>Shadows of Kerr-Sen AdS black hole</b>	<b>6</b>
<b>4</b>	<b>Distortion and energy emission rate: comparative study</b>	<b>9</b>
4.1	Distortion behaviors . . . . .	9
4.2	Energy emission rate . . . . .	10
<b>5</b>	<b>Effects of the cosmological constant on shadows</b>	<b>12</b>
<b>6</b>	<b>Conclusions and discussions</b>	<b>14</b>

## 1 Introduction

Four dimensional black holes have received an increasing interest supported not only by many physical models including superstrings and related theories [1, 2], but also by the international Event Horizon Telescope (EHT) collaboration having unveiled the first shadow image of a supermassive black hole, located in the center of galaxy M87 [3, 4]. A particular emphasis has been put on the interplay between such a physics on Anti-de-Sitter (AdS) geometries with a negative cosmological and thermodynamics. This has opened interesting windows to develop and elaborate many links with critical behaviors appearing in the black hole physics. Concretely, phase transitions of various AdS black holes have been extensively investigated showing non trivial results. In this context, many thermodynamical quantities have been computed in order to unveil the thermodynamical properties of black holes obtained from different gravity theories [5, 6]. Four and higher dimensional concrete solutions have been dealt with by interpreting the cosmological constant as the pressure and its conjugate as the volume [7, 8]. Thermodynamics of charged and rotating (A)dS black hole systems, controlled generally by the mass, the charge and the angular momentum, have been approached using the physics of Van der Waals fluids. Superstring models and M-theory have been also exploited to investigate such properties by implementing other stringy fields including tensor and scalar fields [9–11].

More recently, optical properties of four dimensional black holes have been largely studied in connections with non trivial backgrounds completing the thermodynamical investigations [12, 13]. Precisely, the shadows have been considered as a physical reality supported by EHT collaborations. For such reasons, shadow and deflection angle behaviors of various charged and rotating black holes have been discussed using different methods. In particular, it has been revealed that the shadows of non rotating black holes involve a circular geometry. However, such a geometry can be deformed by introducing rotation parameters needed for engineering spinning solutions. In certain models, the size of such a geometry depends also on certain parameters associated with external sources

including dark energy (DE) and dark matter (DM) [14, 15]. A close inspection shows that the charged rotating (A)dS black hole shadows, in light of observations, could provide insight to the spacetime structure and information on the corresponding physics. In particular, the geodesics can be linked to two-point correlations in AdS/CFT context [16]. Therefore, the analysis of such shadows could be considered as a useful tool to not only explore the astrophysical black holes but also to compare alternative theories with general relativity.

The aim of this work is to investigate the shadow behaviors of four dimensional charged rotating black holes with a cosmological constant in terms of a reduced moduli space parameterized by the charge and the rotation parameters. For AdS backgrounds, we elaborate, in some details, explicit models treating the Kerr-Newman (KN) solution and the Kerr-Sen (KS) black hole obtained more recently in [17]. A key observation is that we find cardioid-like (heart-shaped) shapes. Then, we discuss and compare the geometrical observables and the energy emission rate of both black holes. Inspecting the effect of the cosmological constant, we get constraints generating cardioid-like shadows for (A)dS spaces. Links with other results are also given. In this work, dimensionless units have been used ( $G = \hbar = c = 1$ ).

The paper is structured as follows. In sections 2 and 3, we investigate the shadow behaviors of KN-AdS and KS-AdS black holes with a negative cosmological constant, respectively. Then, certain results and comparative discussions on such behaviors are provided in section 4. In section 5, we inspect the cosmological constant effect on optical aspects for (A)dS backgrounds. The last section is devoted to conclusions and open questions

## 2 Shadows of Kerr-Newman AdS black hole

In this section, we investigate the photon geodesics around the four dimensional KN black hole with a cosmological constant, being a charged generalization of the Kerr black solution. To get such a solution, one should exploit the Einstein-Maxwell modified action which reads as

$$\mathcal{I} = -\frac{1}{16\pi G} \int_M dx^4 \sqrt{-g} [R - F^2 + 2\Lambda] \quad (2.1)$$

where  $F = dA$  denotes the field strength of the gauge potential 1-form.  $\Lambda$  is the cosmological constant. It is worth nothing that two solutions can arise depending on  $\Lambda$ . For  $\Lambda > 0$ , the solution will be called Kerr-Newman de Sitter (KN-dS). However,  $\Lambda < 0$  generates a solution referred to as Kerr-Newman Anti de Sitter (KN-AdS) which will be investigated in certain details trough this work. As usually, the variation of the above action with respect to the metric tensor  $g_{\mu\nu}$  can give KN solutions. According to [18, 19], the Boyer-Lindquist coordinates provide the following line element

$$ds^2 = -\frac{\Delta_r}{\Sigma} \left( dt - \frac{a}{\Xi} \sin^2 \theta d\phi \right)^2 + \Sigma \left( \frac{dr^2}{\Delta_r} + \frac{d\theta^2}{\Delta_\theta} \right) + \frac{\Delta_\theta \sin^2 \theta}{\Sigma} \left( a dt - \frac{(r^2 + a^2)}{\Xi} d\phi \right)^2$$

where one has  $\Sigma = r^2 + a^2 \cos^2 \theta$  and  $\Xi = 1 + \frac{\Lambda}{3} a^2$ . However, the  $\Delta$  functions are given by

$$\Delta_\theta = 1 + \frac{\Lambda}{3} a^2 \cos^2 \theta, \quad \Delta_r = (r^2 + a^2) \left( 1 - \frac{\Lambda r^2}{3} \right) - 2mr + Q^2. \quad (2.2)$$

Here,  $m$ ,  $a$  and  $Q$  are the mass parameter, the angular momentum per unit mass and the charge, respectively. According to shadow black hole activities, the photon equation of motion on such a background can be elaborated using the Hamilton-Jacobi equation

$$\frac{\partial S}{\partial \tau} + \frac{1}{2} g^{\mu\nu} \frac{\partial S}{\partial x^\mu} \frac{\partial S}{\partial x^\nu} = 0, \quad (2.3)$$

where  $\tau$  is the affine parameter associated with the geodesics.  $S$  being known by the Jacobi action is given by

$$S = -Et + L\phi + S_r(r) + S_\theta(\theta), \quad (2.4)$$

where  $E = -p_t$  and  $L = p_\phi$  are the conserved total energy and the conserved angular momentum of the photon, respectively, where  $p_\mu$  is its four-momentum. They are geodesic constants of motion.  $S_r(r)$  and  $S_\theta(\theta)$  are functions depending only on  $r$  and  $\theta$  variables, respectively. To get the complete relations of null geodesics, a separation method is needed which could be supported by the Carter mechanism [20]. The illustration of the black hole shadow geometries requires two dimensionless impact parameters expressed as

$$\xi_{KN} = \frac{L}{E}, \quad \eta_{KN} = \frac{\mathcal{K}}{E^2}, \quad (2.5)$$

where  $\mathcal{K}$  denotes a separable constant analogue to the Carter one reported in [20]. The subscript  $KN$  stands for the KN black hole solution. To obtain the corresponding relations, certain calculations should be performed. Indeed, they give the null geodesics equations

$$\Sigma \frac{dt}{d\tau} = E \left[ \frac{(r^2 + a^2) [(r^2 + a^2) - a\xi_{KN}\Xi]}{\Delta_r} + \frac{a(\xi_{KN}\Xi - a\sin^2\theta)}{\Delta_\theta} \right], \quad (2.6)$$

$$\Sigma \frac{dr}{d\tau} = \sqrt{\mathcal{R}_{KN}(r)}, \quad (2.7)$$

$$\Sigma \frac{d\theta}{d\tau} = \sqrt{\Theta_{KN}(\theta)}, \quad (2.8)$$

$$\Sigma \frac{d\phi}{d\tau} = E \Xi \left[ \frac{a((r^2 + a^2) - a\xi_{KN}\Xi)}{\Delta_r} + \frac{\xi_{KN}\Xi - a\sin^2\theta}{\sin^2\theta \Delta_\theta} \right]. \quad (2.9)$$

In these relations,  $\mathcal{R}_{KN}(r)$  and  $\Theta_{KN}(\theta)$  which describe the radial and the polar motion read as

$$\mathcal{R}_{KN}(r) = E^2 \left[ [(r^2 + a^2) - a\xi_{KN}\Xi]^2 - \Delta_r \left[ \frac{(a - \xi_{KN}\Xi)^2}{\Delta_\theta} + \eta_{KN} \right] \right], \quad (2.10)$$

$$\Theta_{KN}(\theta) = E^2 \left[ \eta_{KN} \Delta_\theta - \cos^2\theta \left( \frac{\xi_{KN}^2 \Xi^2}{\sin^2\theta} - a^2 \right) \right]. \quad (2.11)$$

It is known that the unstable circular orbit can determine the boundary of the black hole geometric shapes using the constraints

$$\mathcal{R}_{KN}(r) \Big|_{r=r_0} = \frac{d\mathcal{R}_{KN}(r)}{dr} \Big|_{r=r_0} = 0, \quad (2.12)$$

where  $r_0$  represents the circular orbit radius of the photon. After calculations, we find

$$\eta_{KN} = \frac{r^2 \left( 16a^2 \Delta_r \Delta_\theta - (r \Delta'_r - 4\Delta_r)^2 \right)}{a^2 \Delta_\theta \Delta_r'^2} \Big|_{r=r_0}, \quad (2.13)$$

$$\xi_{KN} = \frac{(r^2 + a^2) \Delta'_r - 4r \Delta_r}{a \Xi \Delta'_r} \Big|_{r=r_0}, \quad (2.14)$$

where one has used  $\Delta'_r = \frac{\partial \Delta_r}{\partial r}$ . An examination shows that the boundary of shadows of such black holes depends on many parameters including cosmological constant numerical values. For simplicity reasons, we first consider the AdS backgrounds for which  $\Lambda$  is linked to the characteristic length scale of the AdS geometry via  $\Lambda = -\frac{3}{\ell_{AdS}^2}$ . Results associated with a positive cosmological constant describing dS geometries will be shortly discussed later on. For later use, we introduce a twist charge parameter  $b = Q^2/2m$  in the associated  $\Delta_r$  function. In this way, the shadow geometry will be controlled by a moduli space parameterized by  $\{m, a, b\}$ . Fixing the mass, such a space reduces to  $\{a, b\}$ . To visualise the shadows, we place the observatory in the equatorial plane  $\theta = \pi/2$ .<sup>1</sup> For such a position, we find

$$\eta_{KN} = \frac{r_0^2 (-a^4 r_0^4 + 2a^2 \ell_{AdS}^2 (-4bm (\ell_{AdS}^2 + r_0^2) + 2\ell_{AdS}^2 m r_0 + r_0^3 (3m + r_0)) - A_{KN}^2)}{a^2 B_{KN}^2}, \quad (2.15)$$

$$\xi_{KN} = \frac{\ell_{AdS}^2 (-a^4 r_0 + a^2 (\ell_{AdS}^2 (m + r_0) - r_0^3) + A_{KN} r_0)}{a (a^2 - \ell_{AdS}^2) B_{KN}}, \quad (2.16)$$

where  $A_{KN}$  and  $B_{KN}$  are expressed as follows

$$A_{KN} = \ell_{AdS}^2 (4bm + r_0(r_0 - 3m)), \quad (2.17)$$

$$B_{KN} = r_0 (a^2 + 2r_0^2) + \ell_{AdS}^2 (r_0 - m). \quad (2.18)$$

Considering the limit  $\Lambda = 0$  and  $b = 0$ , these equations become

$$\eta_K = \frac{r_0^3 (4a^2 m - r_0 (3m - r_0)^2)}{a^2 (r_0 - m)^2}, \quad (2.19)$$

$$\xi_K = \frac{r_0^2 (3m - r_0) - a^2 (m + r_0)}{a (r_0 - m)}, \quad (2.20)$$

recovering the results associated with the Kerr black hole reported in [21]. Sending  $a$  to zero, we obtain the Schwarzschild black hole, where the photon sphere can be described by the equation  $\eta_S + \xi_S^2 = 27m$  with  $r_0 = 3m$  [22]. It has been shown that the shadows can be nicely described using the celestial coordinates  $\alpha$  and  $\beta$  developed in many places including [23]. In the present model, they take the following forms

$$\alpha_{KN} = -\xi_{KN} \quad (2.21)$$

$$\beta_{KN} = \pm \sqrt{\eta_{KN}} \quad (2.22)$$

where the observer is placed in the equatorial plane. In Fig.1, the associated shadows are plotted in such a plane by exploiting  $\eta_{KN}$  and  $\xi_{KN}$  expressions. In particular, we illustrate the shadow geometrical behaviors in terms of the  $(a, b)$  reduced moduli space. It has been observed that for very small values of the rotating parameter  $a$  the shadow shape involves a perfect circular geometry. When such a rotation parameter becomes relevant, the black hole develops a so-called D-shape shadow. Increasing the values of  $a$  and the charge parameter  $b$ , the shadow gets a new deformation. In particular, it exhibits cardioid-like (heart-shaped) geometry. Fixing the rotation parameter  $a$ , the shadow size is decreased by the increase of the parameter  $b$ .

---

<sup>1</sup>Other observer positions could be possible which are left for other investigations.

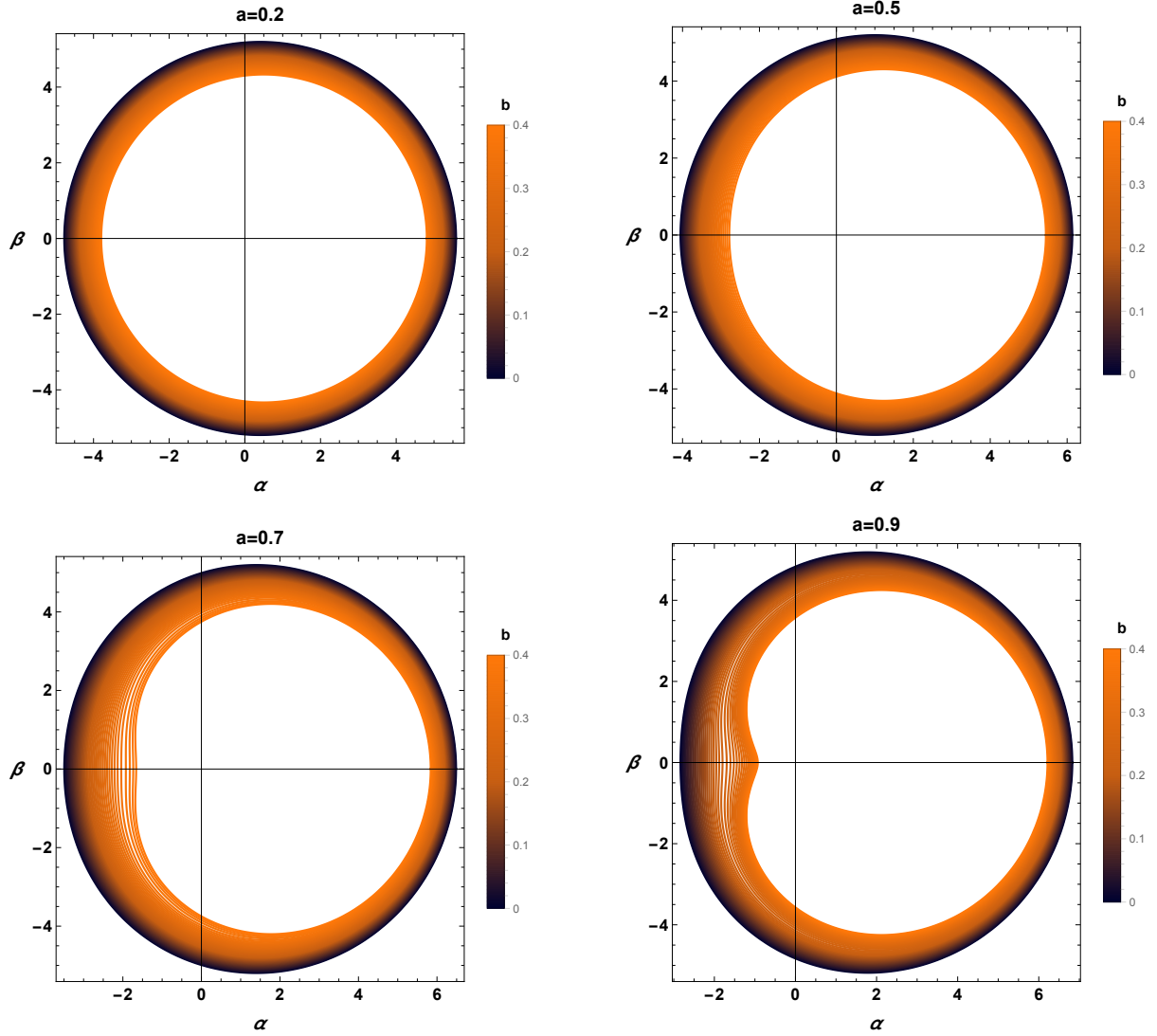


Figure 1: *Shadow behaviors KN-AdS black holes for different values of  $a$  and  $b$  by taking  $\Lambda = -3/\ell^2 = -10^{-4}$  and  $m = 1$ .*

### 3 Shadows of Kerr-Sen AdS black hole

In this section, we deal with the shadow behaviors of the Kerr-Sen black hole with a negative cosmological constant built recently in [17]. We refer to this solution as KS-AdS. This solution has been obtained from the original KS model by implementing a nonzero negative cosmological constant [24]. It is known that this could be derived from a lower energy limit of the heterotic superstring theory living in ten dimension. Concretely, the associated black hole metric can be obtained from an action involving stringy fields, including the dilaton-axion field, a Maxwell field and the B-field. More details on the performed calculations can be found in [24]. Following [17],

the line element the four dimensional KS-AdS black hole, in the coordinates  $(t, r, \theta, \phi)$ , reads as

$$ds^2 = -\frac{\Delta_r}{\Sigma} \left( dt - \frac{a}{\Xi} \sin^2 \theta d\phi \right)^2 + \Sigma \left( \frac{dr^2}{\Delta_r} + \frac{d\theta^2}{\Delta_\theta} \right) + \frac{\Delta_\theta \sin^2 \theta}{\Sigma} \left( a dt - \frac{(r^2 + 2br + a^2)}{\Xi} d\phi \right)^2, \quad (3.1)$$

where the involved terms are given by

$$\Delta_r = (1 + \frac{r^2 + 2br}{\ell_{AdS}^2})(r^2 + 2br + a^2) - 2mr, \quad \Delta_\theta = 1 - \frac{a^2}{\ell_{AdS}^2} \cos^2 \theta, \quad (3.2)$$

$$\Xi = 1 - \frac{a^2}{\ell_{AdS}^2}, \quad \Sigma = r^2 + 2br + a^2 \cos^2 \theta. \quad (3.3)$$

It is indicated that  $m$  is a mass function and where  $a$  is a rotating parameter as before. While, the parameter  $b$  given  $b = Q^2/2m$  denotes now the dilatonic scalar charge, playing the same role as the charge parameter of the KN black hole solution given in Eq.(2.2). Using similar techniques, the first-order differential equations, describing the photon motion in such a background, read as

$$\Sigma \frac{dt}{d\tau} = E \left[ \frac{(r^2 + 2br + a^2) [(r^2 + 2br + a^2) - a\xi_{KS}\Xi]}{\Delta_r} + \frac{a (\xi_{KS}\Xi - a \sin^2 \theta)}{\Delta_\theta} \right], \quad (3.4)$$

$$\Sigma \frac{dr}{d\tau} = \sqrt{\mathcal{R}_{KS}(r)}, \quad (3.5)$$

$$\Sigma \frac{d\theta}{d\tau} = \sqrt{\Theta_{KS}(\theta)}, \quad (3.6)$$

$$\Sigma \frac{d\phi}{d\tau} = E \Xi \left[ \frac{a((r^2 + 2br + a^2) - a\xi_{KS}\Xi)}{\Delta_r} + \frac{\xi_{KS}\Xi - a \sin^2 \theta}{\sin^2 \theta \Delta_\theta} \right]. \quad (3.7)$$

In these equations,  $\mathcal{R}_{KS}(r)$  and  $\Theta_{KS}(\theta)$  describing the radial and the polar motion take the following form

$$\mathcal{R}_{KS}(r) = E^2 \left[ [(r^2 + 2br + a^2) - a\xi_{KS}\Xi]^2 - \Delta_r \left[ \frac{(a - \xi_{KS}\Xi)^2}{\Delta_\theta} + \eta_{KS} \right] \right], \quad (3.8)$$

$$\Theta_{KS}(\theta) = E^2 \left[ \eta_{KS} \Delta_\theta - \cos^2 \theta \left( \frac{\xi_{KS}^2 \Xi^2}{\sin^2 \theta} - a^2 \right) \right]. \quad (3.9)$$

Imposing the constraints  $\mathcal{R}_{KS}(r)|_{r=r_0} = \frac{d\mathcal{R}_{KS}(r)}{dr}|_{r=r_0} = 0$ , the shadow behaviors of the KS-AdS black hole can be determined by the following impact parameters

$$\eta_{KS} = \frac{16(b+r)^2 \Delta(r) (a^2 \Delta(\theta) - \Delta_r) + r(2b+r) \Delta'(r) (8(b+r) - r(2b+r) \Delta'(r))}{a^2 \Delta(\theta) \Delta'(r)^2} \Big|_{r=r_0} \quad (3.10)$$

$$\xi_{KS} = \frac{a^2 \Delta'(r) + 2br \Delta'(r) - 4b \Delta(r) + r^2 \Delta'(r) - 4r \Delta(r)}{a \Xi \Delta'(r)} \Big|_{r=r_0}. \quad (3.11)$$

Placing the observatory in the equatorial plane  $\theta = \pi/2$ , these two equations reduce to

$$\eta_{KS} = \frac{r_0^2 \left( -a^4 (2b^2 + 3br_0 + r_0^2)^2 + 2a^2 \ell_{AdS}^2 (b + r_0) C_{KS} - A_{KS}^2 \right)}{a^2 B_{KS}^2} \quad (3.12)$$

$$\xi_{KS} = \frac{\ell_{AdS}^2 \left( -a^4 (b + r_0) + a^2 (-2b^2 r_0 + b (\ell_{AdS}^2 - 3r_0^2) + \ell_{AdS}^2 (m + r_0) - r_0^3) + r_0 A_{KS} \right)}{a B_{KS}}, \quad (3.13)$$

where  $A_{KS}$ ,  $B_{KS}$ , and  $C_{KS}$  are expressed as follows

$$A_{KS} = \ell_{AdS}^2(2b^2 - 2bm + 3br_0 - 3mr_0 + r_0^2), \quad (3.14)$$

$$B_{KS} = a^2(b + r_0) + 4b^2r_0 + b(\ell_{AdS}^2 + 6r_0^2) - \ell_{AdS}^2m + \ell_{AdS}^2r_0 + 2r_0^3, \quad (3.15)$$

$$C_{KS} = 4b^3 + 4b^2(m + 2r_0) + br_0(8m + 5r_0) + 2\ell_{AdS}^2m + r_0^2(3m + r_0). \quad (3.16)$$

Taking the limit  $\ell_{AdS}$  goes to the infinity, we recover the usual the KS black hole equations [25]. In order to visualise the shadows of KS-AdS black hole, we introduce the celestial coordinates  $\alpha_{KS}$  and  $\beta_{KS}$  in the equatorial plane as in the previous model. The corresponding behaviors in terms of the  $(a, b)$  reduced moduli space are plotted in Fig.2. It follows from such a figure that

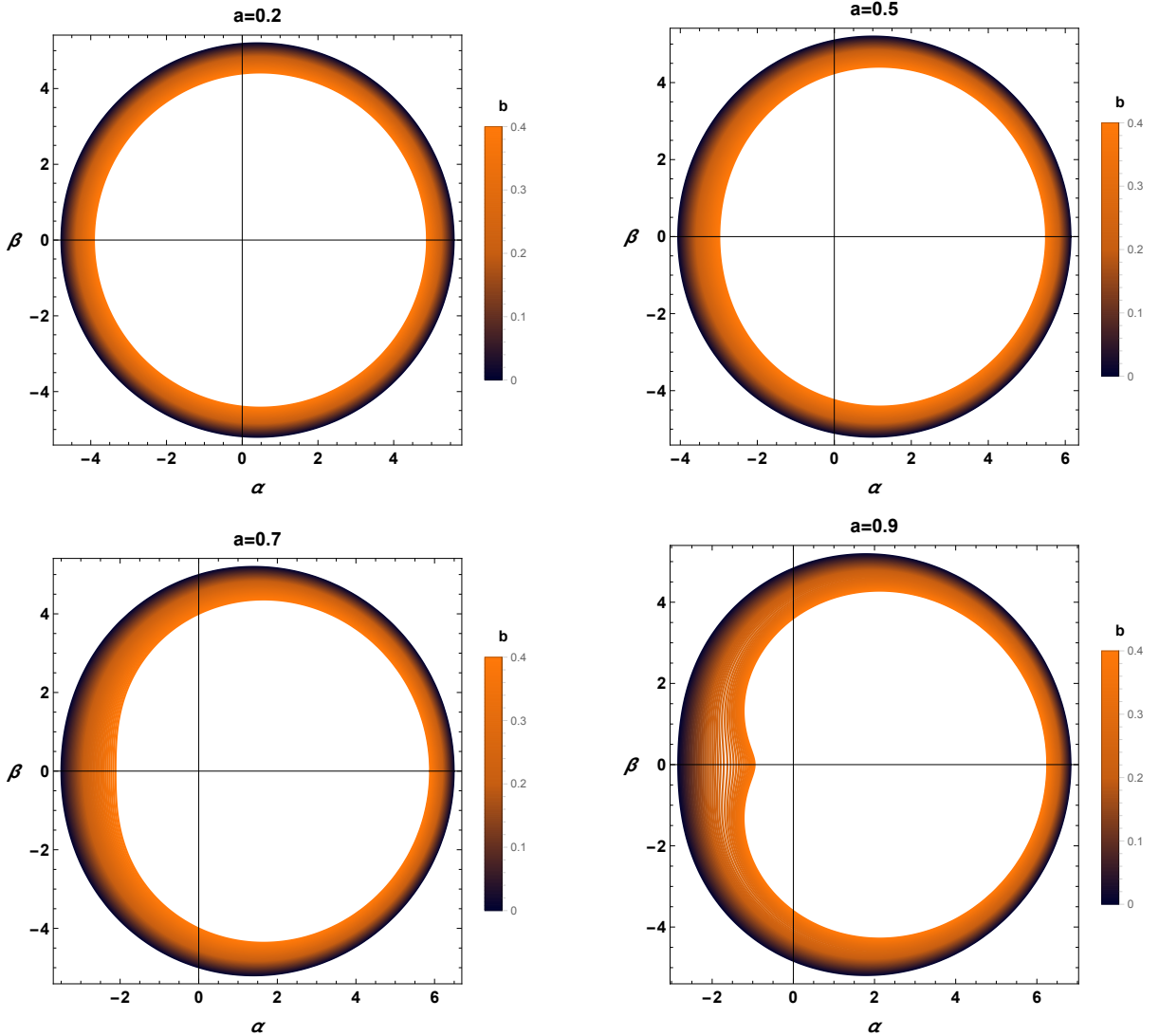


Figure 2: *Shadow behaviors KS-AdS black holes for different values of  $b$  and  $a$  by considering  $\Lambda = -3/\ell^2 = -10^{-4}$  and  $m = 1$ .*

the shadow shape is circular for slowly rotating black hole solutions. Moreover, its size depends on



the  $b$  parameter. Indeed, it decreases by increasing  $b$ . For the values of  $a$  close to 0.9, an identical behavior associated with cardioid-like shapes has been remarked passing by a D-shape observed near  $a = 0.7$ . A close inspection relying on known result pushes one to suggest that the presence of the charge parameter has considerable effects on the black hole silhouette being heart-shaped. This suggestion needs deeper reflections being left for other investigations. The size gets smaller by increasing such a parameter. We expect that the shadows shrink for very large values of  $b$ .

## 4 Distortion and energy emission rate: comparative study

In this section, we would like to provide a comparative study associated with a negative cosmological constant using certain regions of the  $(a, b)$  reduced moduli space. First, we start with the geometrical distortion behaviors. Then, we deal with the energetic aspects by examining the energy emission rate.

### 4.1 Distortion behaviors

To inspect the geometric deformations of the black hole shadows, one usually need two parameters  $R_c$  and  $\delta_c$  controlling the size and the shape, respectively [26, 27]. In particular, the size is characterized by three specific points being top and bottom position of shadow  $(\alpha_t, \beta_t)$ ,  $(\alpha_b, \beta_b)$ , the point of reference circle  $(\tilde{\alpha}_p, 0)$ . The point of distorted shadow circle  $(\alpha_p, 0)$  intersects the horizontal axis at  $\alpha_p$ . The distance between the two latter points is controlled by a parameter  $D_c = \tilde{\alpha}_p - \alpha_p = 2R_c - (\alpha_r - \alpha_p)$  [27]. Indeed, the parameter  $R_c$  of the shadow is approximately given by

$$R_c = \frac{(\alpha_t - \alpha_r)^2 + \beta_t^2}{2|\alpha_t - \alpha_r|}. \quad (4.1)$$

However, the distortion parameter defined as a ratio of  $D_c$  and  $R_c$  reads as

$$\delta_c = \frac{D_c}{R_c}. \quad (4.2)$$

To provide a deep comparative study concerning the KN-AdS and the KS-AdS black holes, we analyse the astronomical parameters  $R_c$  and  $\delta_c$ . These two observables are plotted in left panels of Fig.3 in terms of the  $(a, b)$  reduced moduli space. It has been observed that  $R_c$ , controlling the size, decreases by increasing the parameters  $b$ . For values of  $b$  between 0 and 0.15,  $R_c$  is almost the same for both black holes even if we vary the parameter  $a$ . For  $b > 0.15$ ,  $R_c^{KS}$  is bigger than  $R_c^{KN}$  for different values of  $a$ . Concerning the remaining astronomical parameter  $\delta_c$ , controlling the distortion, it is plotted for both black holes in right panels of Fig.3. It follows that for  $a = 0.1$ , the distortion parameter  $\delta_c$  is almost zero for both types of black holes. For  $a > 0.1$ ,  $\delta_c$  increases by increasing the parameter  $a$ . It has been observed that  $\delta_c^{KN}$  is bigger than  $\delta_c^{KS}$  for values of  $b$  above 0.2. For values lower than 0.2, however,  $\delta_c^{KN}$  and  $\delta_c^{KS}$  are equal. For  $b = 0.1$ , the distortion  $\delta_c$  of the two black holes coincides even if we vary the parameter  $a$ . Otherwise,  $\delta_c^{KN}$  is bigger than  $\delta_c^{KS}$ , showing that the distortion in the KN-AdS spacetime is more relevant than the one in the KS-AdS background.

Having discussed the shadow shapes of the rotating and charged black holes with a negative cosmological constant, we move to investigate the energy emission rate.

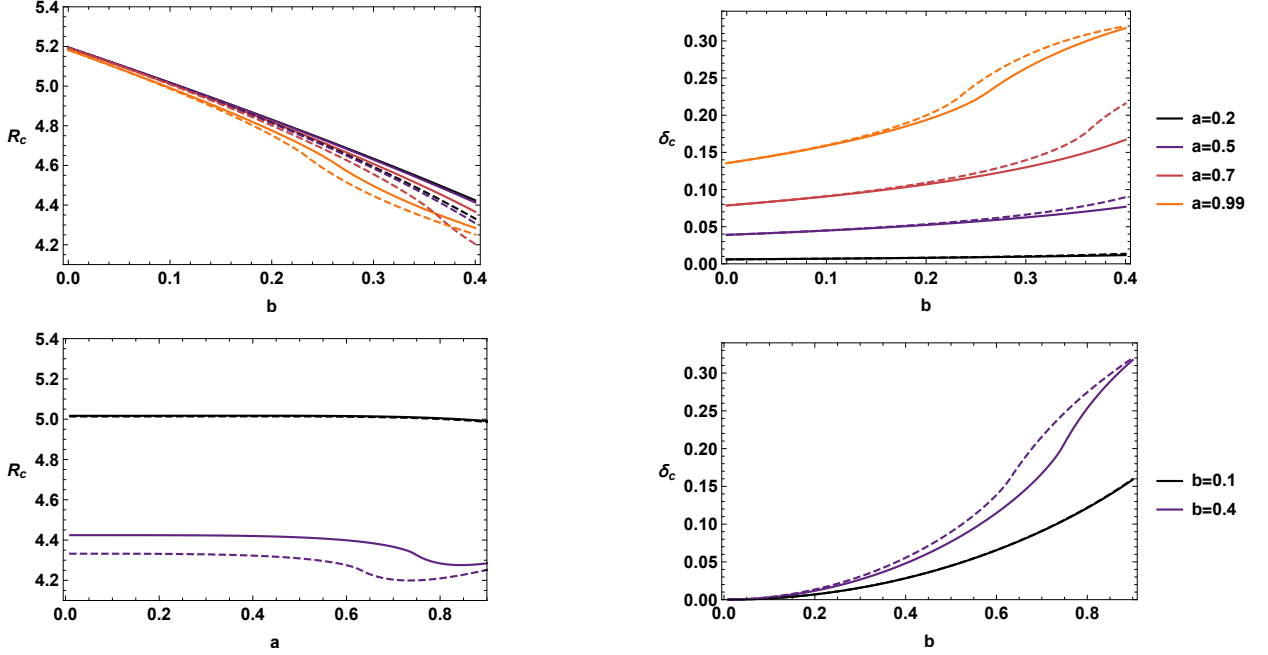


Figure 3: Astronomical observables for different values of  $b$  and  $a$  by taking  $\Lambda = -3/\ell^2 = -10^{-4}$  and  $m = 1$ . Dashed lines represent KN-AdS black holes and the continuous ones represent KS-AdS black holes.

## 4.2 Energy emission rate

It has been known that for, a far distant observer, the absorption cross-section approaches to the black hole shadow. At very high energy, it is noted that the absorption cross-section oscillates near to a limiting constant value. According to [28], the later being approximately equal to the area of the photon sphere ( $\sigma \sim \pi R_c^2$ ) provides the energy emission rate expression given by

$$\frac{d^2 E(\varpi)}{d\varpi dt} = \frac{2\pi^3 (R_c^i)^2}{e^{\frac{\varpi}{T_i}} - 1} \varpi^3, \quad i = KN, KS \quad (4.3)$$

where  $\varpi$  is the emission frequency. In this relation,  $T_i$  which denote the temperature of the four-dimensional rotating and charged AdS black holes, which can be given in terms of the horizon radius  $r_h^i$  ( $\Delta_r(r_h^i) = 0$ ). It has been observed that not all values of the temperature and the horizon radius are allowed for the the rotating AdS black hole due to the presence of the parameter  $a$  in the involved expressions. For the KS-AdS black hole, the temperature reads as

$$T_{KS} = \frac{1}{2\pi (a^2 + (r_h^{KS})^2)} \left( \frac{(b + r_h^{KS}) (a^2 + 4br_h^{KS} + 2(r_h^{KS})^2)}{\ell_{AdS}^2} - m + b + r_h^{KS} \right). \quad (4.4)$$

In Fig.4, we plot the energy emission rate as a function of the emission frequency  $\varpi$  for certain points of the  $(a, b)$  moduli space.

It has been remarked from such a figure that the effect of the twist parameter  $b$  changes when we increase the rotation rate  $a$ . For  $a = 0.2$ , we concretely observe that the energy emission rate increases with the increase in the value of the parameter  $b$ . For  $a = 0.9$ , however, an opposite

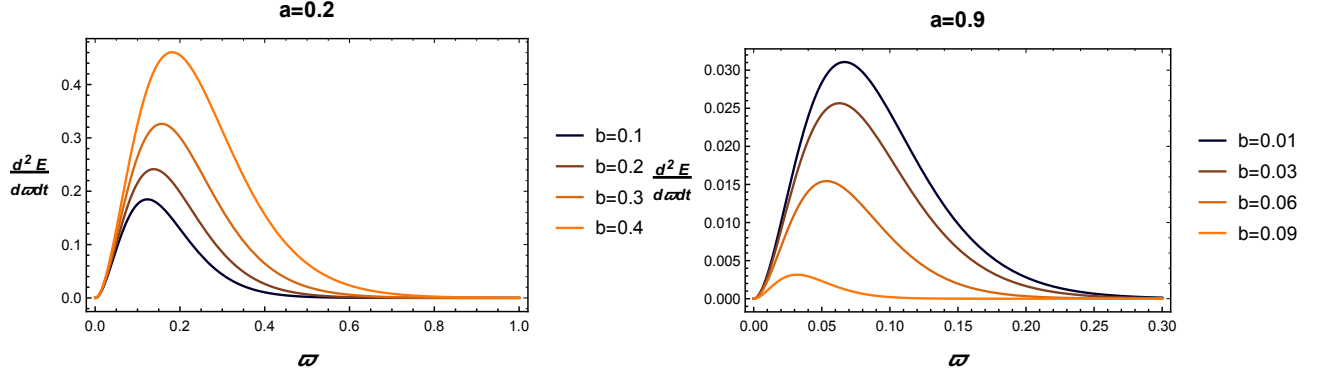


Figure 4: Energy Emission rate for KS-AdS black hole for different values of  $b$  and  $a$ .

behavior is observed. Moreover, we notice that the emission rate decreases by increasing the parameter  $a$ .

For KN-AdS black hole, certain distinctions appear. Indeed, the Hawking temperature is given by

$$T_{KN} = \frac{1}{2\pi (a^2 + (r_h^{KN})^2)} \left( \frac{r_h^{KN} (a^2 + 2(r_h^{KN})^2)}{\ell_{AdS}^2} - m + r_h^{KN} \right). \quad (4.5)$$

It has been observed that when we increase the rotation parameter  $a$ , some constraints are imposed on the parameter  $b$ . In fact, only the small values of the latter are possible being also seen for the horizon radius  $r_h^{KN}$ . For such regions, the energy emission rate can be approached. In Fig.5, these energetic aspects are plotted as a function of the emission frequency  $\omega$  for different values of  $a$  and  $b$ .

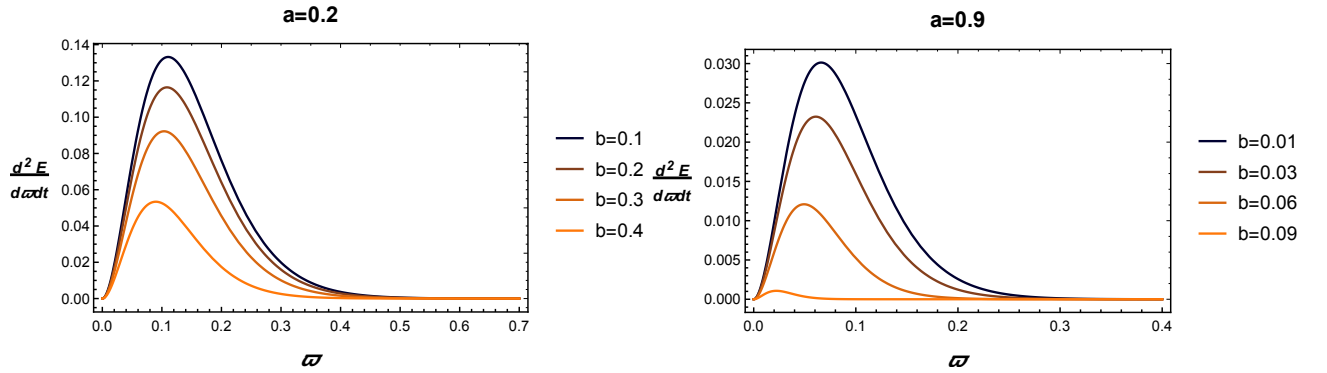


Figure 5: Energy emission rate of KN-AdS black hole for different values of  $b$  and  $a$ .

For small values of the rotation rate  $a$ , it has been seen from this figure that the KN-AdS black hole involves a slower evaporation process contrary to the KS-AdS one. Increasing the rotation rate parameter  $a$ , however, we remark that both black holes exhibit similar behaviors. A particular observation is that when we increase  $b$ , the KN emission rate becomes smaller than the KS one

which can be clearly observed from the associated shadow radius and the temperature. This could be due to stringy effects on the black hole solutions. This suggestion could be addressed in future works.

## 5 Effects of the cosmological constant on shadows

In this section, we inspect the effects of the cosmological constant on shadows for both classes of charged rotating black holes. In Fig.6, shadows with negative and positive cosmological constant values for KN-(A)dS are compared at particular point of the reduced moduli space. It follows from this figure that the shadow size is larger for the dS geometry.

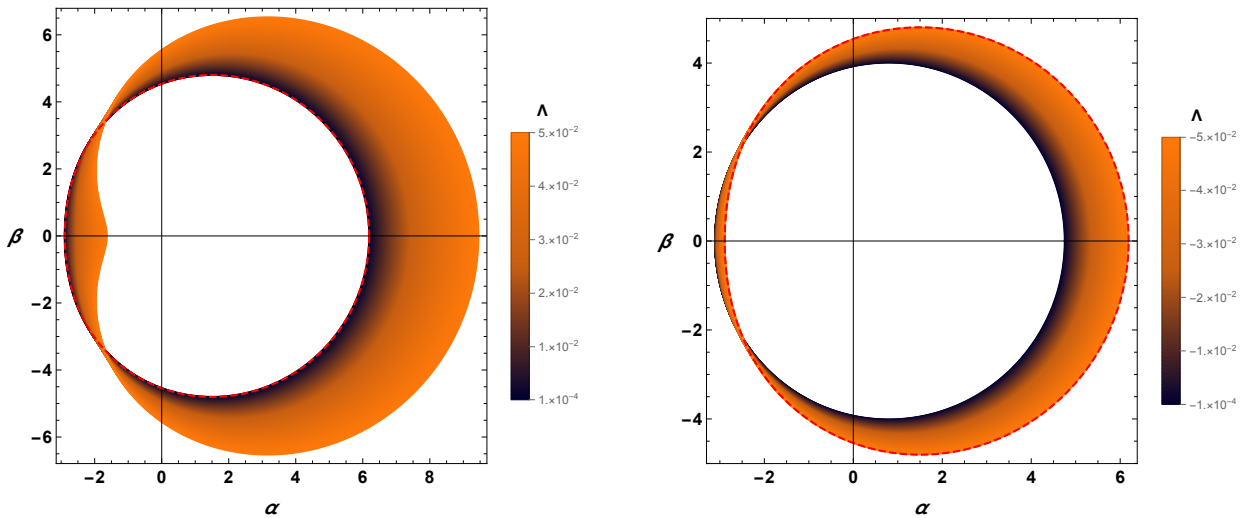


Figure 6: Shadow behaviors for KN-AdS for different values of the cosmological constant  $\Lambda$ , for  $a = 0.7$ ,  $b = 0.2$  and  $m = 1$ . In all panels, the red and dashed lines correspond to  $\Lambda = 0$ .

Besides, we observe from Fig.6 that the cardioid-like shadow appear for smaller values of the parameters  $(a, b)$  in the dS background contrary to the AdS one. For fixed values of the parameters  $(a, b)$ , we compare the case of  $\Lambda = 0$  with AdS and dS backgrounds. In particular, we find that the former presence decreases the shadow size, while the latter increases it. This figure also reveals that for the particular numerical value  $\Lambda = 5 \cdot 10^{-2}$  we can observe the cardioid-like shape. Thus, we can conclude that the positive values of the cosmological constant (de Sitter space) can be considered as a boost to the shadow distortion. This result has been confirmed for KS-(A)dS illustrated in Fig.7. A close inspection shows that there is a link between the cardioid-like shape and the impact parameters  $\eta_i$  and  $\xi_i$ . Inspired by results of shadow figures, it has been concluded that such a link is translated to a requirement on  $\eta_i$  and  $\xi_i$ . For the usual shadow form, the condition is given by

$$|\eta_i| \geq 2\lambda_i \quad (5.1)$$

where  $\lambda_i = ||\eta_i| - |\xi_i||$ . The the cardioid-like shadow shape, however, is associated with

$$\lambda_i < |\eta_i| < 2\lambda_i. \quad (5.2)$$

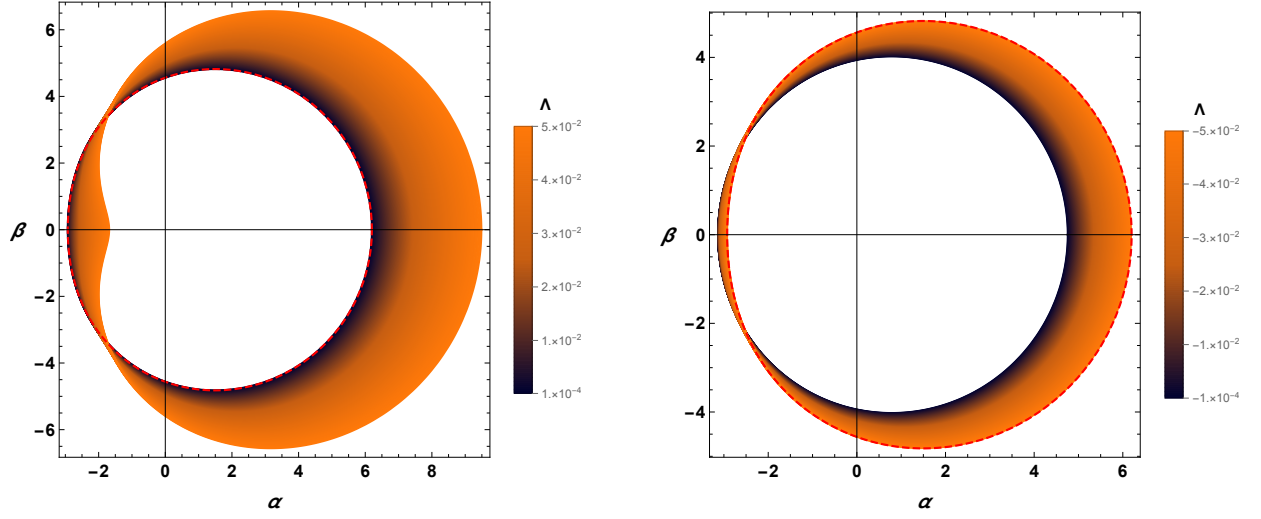


Figure 7: *Shadow behaviors for KS-AdS for different values of cosmological constant  $\Lambda$  for  $a = 0.7$ ,  $b = 0.2$  and  $m = 1$ . In all panels, the red and dashed lines are associated with  $\Lambda = 0$ .*

For such conditions, the observables are examined as illustrated in Fig.8. It has been observed that such optical quantities are the same for positive and negative cosmological constant. An examination shows that the previous finding is also confirmed even for dS geometries. Moreover, a similar comparative discussion has been elaborated for zero cosmological constant at generic points of the moduli space [29]. For small parameter values, we find the same result. It should be interesting to check others regions which could involve non trivial distinctions originated from stringy behaviors of black holes.

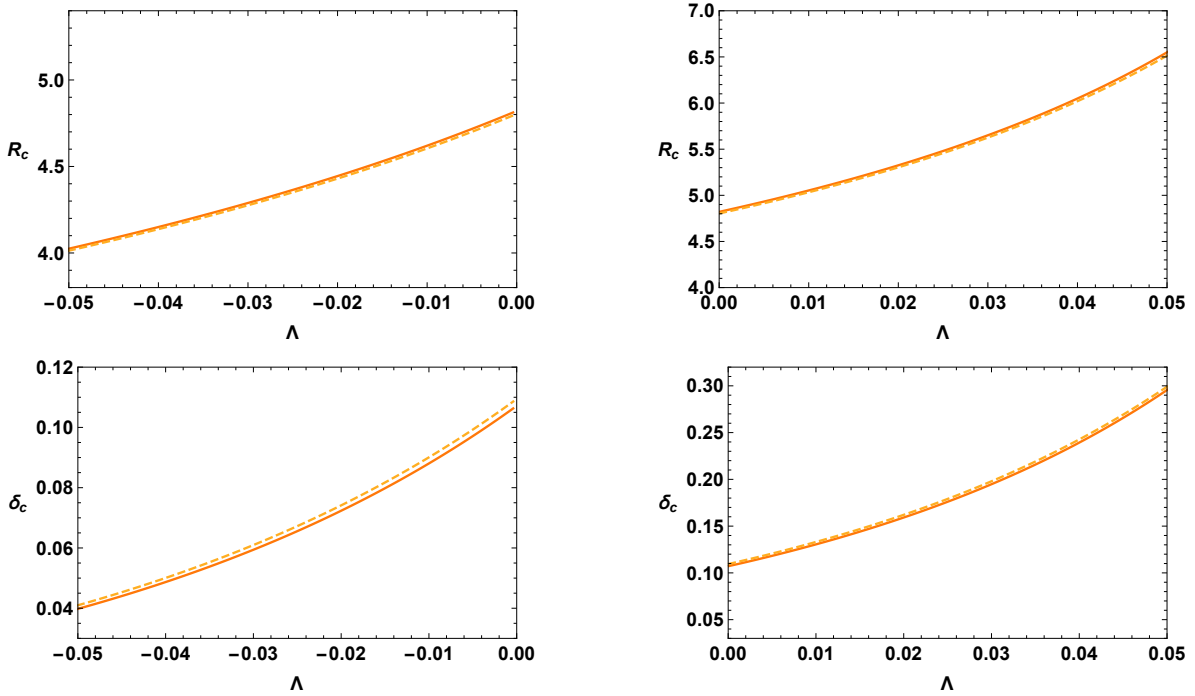


Figure 8: *Astronomical observable for different values of cosmological constant  $\Lambda$ , for  $a = 0.7$ ,  $b = 0.2$  and  $m = 1$ . Dashed and continuous lines represent KN-AdS and KS-AdS respectively.*

## 6 Conclusions and discussions

More recently, it has been remarked that the shadows of black holes has been considered as an active research subject encouraged by the finding of ETH international collaborations. Motivated by such activities, we have investigated the shadows of charged rotating black holes with a cosmological constant. For AdS geometries, we have elaborated two explicit models. First, we have studied shadow optical behaviors of the KN-AdS black hole. Then, we have dealt with the KS-AdS black hole built recently in [17]. The key observation is that the shadows of both black holes exhibit cardioid-like shapes for particular regions of the  $(a, b)$  moduli space. In order to unveil more data on such optical behaviors of charged rotating black holes with a negative cosmological constant, we have provided a comparative study. Precisely, we have found that the KN-AdS black hole possesses a shadow radius less important than the KS-AdS one. However, the distortion is more relevant in the KN-AdS background. These optical aspects have been consolidated by the energy emission rate and evaporation process. In such an investigation, relevant distinctions have appeared. Precisely, the KN-AdS energy emission rate is small compared to the KS-AdS one for some regions of the reduced moduli space  $(a, b)$ . Moreover, we have noticed that certain  $(a, b)$  regions have different effects on the KN-AdS black hole compared to the KS-AdS one. An opposite behavior of the parameter  $b$  for the slow rotation rate has been observed. Inspecting the effects of the cosmological constant on the studied black holes, we have found the moduli space regions favoring cardioid-like shadows for (A)dS backgrounds.

This paper comes up with many questions. It would be of interest to inspect behaviors associated with non trivial backgrounds by considering either the effects of the spacetime dimension or external sources provided by DE and DM. It should be also interesting to make contact with theoretical and observational findings. We hope to address elsewhere these open questions.

## Acknowledgment

The authors would like to thank K. Masmar, M. B. Sedra and E. Torrente-Lujan for discussions on related topics. This work is partially supported by the ICTP through AF-13.

## References

- [1] S. W. Hawking, *Black holes in general relativity*, *Communications in Mathematical Physics* **25**(2) (1972) 152-166.
- [2] A. Strominger, C. Vafa, *Microscopic origin of the Bekenstein-Hawking entropy*, *Phys. Lett. B* **379** (2019) 99.
- [3] K. Akiyama *et al.* [Event Horizon Telescope], *First M87 Event Horizon Telescope Results. I. The Shadow of the Supermassive Black Hole*, *Astrophys. J.* **875**, no.1, L1 (2019), arXiv:1906.11238 [astro-ph.GA].
- [4] K. Akiyama *et al.* [Event Horizon Telescope], *First M87 Event Horizon Telescope Results. IV. Imaging the Central Supermassive Black Hole*, *Astrophys. J. Lett.* **875**, no.1, L4 (2019), arXiv:1906.11241 [astro-ph.GA].
- [5] N. Altamirano, D. Kubiznak, R. B. Mann, Z. Sherkatghanad, *Thermodynamics of rotating black holes and black rings: phase transitions and thermodynamic volume*, *Galaxies* **2** (2014) 89-159, arXiv:1401.2586 [hep-th].
- [6] A. Belhaj, M. Chabab, H. El Moumni, M. B. Sedra, *On Thermodynamics of AdS Black Holes in Arbitrary Dimensions*, *Chin. Phys. Lett.* **29** (2012)100401, arXiv:1210.4617 [hep-th].
- [7] B. P. Dolan, *Pressure and volume in the first law of black hole thermodynamics*, *Class. Quant. Grav.* **28** (2011) 235017, arXiv:1106.6260 [gr-qc].
- [8] D. Kubiznak, R. B. Mann, *P-V criticality of charged AdS black holes*, *J. High Energy Phys.* **1207** (2012) 033.
- [9] J. L. Zhang, R. G. Cai, H. Yu, *Phase transition and thermodynamical geometry for Schwarzschild AdS black hole in  $AdS^5 \times S^5$  spacetime*, *J. High Ener. Phys.* **2** (2015) 143.
- [10] A. Belhaj, M. Chabab, H. El Moumni, K. Masmar, M. B. Sedra, *On thermodynamics of AdS black holes in M-theory*, *Eur. Phys. J. C* **76**(2) (2016) 73.
- [11] A. Belhaj, A. El Balali, W. El Hadri, Y. Hassouni, E. Torrente-Lujan, *Phase Transitions of Quintessential AdS Black Holes in M-theory/Superstring Inspired Models*, arXiv:2004.10647.

- [12] M. Zhang, M. Guo, *Can shadows reflect phase structures of black holes?*, arXiv:1909.07033 [gr-qc].
- [13] A. Belhaj, L. Chakhchi, H. El Moumni, J. Khalloufi, K. Masmar, *Thermal Image and Phase Transitions of Charged AdS Black Holes using Shadow Analysis*, arXiv:2005.05893 [gr-qc].
- [14] A. Abdujabbarov, B. Toshmatov, Z. Stuchlik, B. Ahmedov, *Shadow of the rotating black hole with quintessential energy in the presence of plasma*, Int. J. Mod. Phys. D **26**, no.06, (2016) 1750051, arXiv:1512.05206.
- [15] S. Haroon, M. Jamil, K. Jusufi, K. Lin, R. B. Mann, *Shadow and Deflection Angle of Rotating Black Holes in Perfect Fluid Dark Matter with a Cosmological Constant*, Phys. Rev. D **99** (2019) 044015.
- [16] V. Balasubramanian, S. F. Ross, *Holographic particle detection*, Phys. Rev. D **61**(2000) 044007, arXiv:hep-th/9906226 [hep-th].
- [17] D. Wu, P. Wu, H. Yu, S. Q. Wu, *Are ultra-spinning Kerr-Sen-AdS<sub>4</sub> black holes always super-entropic ?*, arXiv:2007.02224 [gr-qc].
- [18] B. Carter, *Hamilton-Jacobi and Schrodinger separable solutions of Einstein's equations*, Commun. Math. Phys. **10** (1968) 280.
- [19] J. F. Plebanski, M. Demianski, *Rotating, charged, and uniformly accelerating mass in general relativity*, Ann. Phys. **98** (1976) 98–127.
- [20] B. Carter, *Global structure of the kerr family of gravitational fields*. Physical Review, **174**(5) (1968)1559.
- [21] S. W. Wei, Y. C. Zou, Y. X. Liu, R. B. Mann, *Curvature radius and Kerr black hole shadow*, JCAP **08**, (2019)030, arXiv:1904.07710 [gr-qc].
- [22] H. Lu, H. D. Lyu, *Schwarzschild black holes have the largest size*, Phys. Rev. D **101**, no.4, (2020)044059, arXiv:1911.02019 [gr-qc].
- [23] C. Subrahmanyam, *The mathematical theory of black holes*, volume 69. Oxford University Press, 1998.
- [24] A. Sen, *Rotating charged black hole solution in heterotic string theory*, Phys. Rev. Lett. **69**(7) (1992) 1006.
- [25] X. G. Lan, J. Pu, *Observing the contour profile of a Kerr–Sen black hole*, Mod. Phys. Lett. A **33**, no.17, (2018) 1850099.
- [26] K. Hioki, K. I. Maeda, *Measurement of the kerr spin parameter by observation of a compact object's shadow*, Phys. Rev. D, **80**(2)(2009)024042 .
- [27] M. Amir, S. G Ghosh, *Shapes of rotating nonsingular black hole shadows*, Phys. Rev. D **94**(2) (2016) 024054.



- [28] S. W. Wei, Y. X. Liu, *Observing the shadow of Einstein-Maxwell-Dilaton-Axion black hole*, JCAP **11** (2013)063, arXiv:1311.4251 [gr-qc].
- [29] S. V. M. C. B. Xavier, Pedro V. P. Cunha, Luís C. B. Crispino, Carlos A. R. Herdeiro, *Shadows of charged rotating black holes: Kerr-Newman versus Kerr-Sen*, arXiv:2003.14349.